ARMY RESEARCH LABORATORY

Low-Cost Conical Ultra-Wideband Antenna

by Eric E. Funk and Stephen E. Saddow

ARL-TR-302 November 1994

The findings in this report are not to be construed as an official Department of the Army position unless so designated by other authorized documents.

Citation of manufacturer's or trade names does not constitute an official endorsement or approval of the use thereof.

Destroy this report when it is no longer needed. Do not return it to the originator.

REPORT DOCUMENTATION PAGE

Form Approved
OMB No. 0704-0188

1. AGENCY USE ONLY (Leave blank)	2. REPORT DATE	3. REPORT TYPE AND DATES COVERED
	November 1994	Final, from May 94–June 94

4. TITLE AND SUBTITLE
Low-Cost Conical Ultra-Wideband Antenna

5. FUNDING NUMBERS
PE: 62120

6. AUTHOR(S)
Eric E. Funk and Stephen E. Saddow

7. PERFORMING ORGANIZATION NAME(S) AND ADDRESS(ES)
U.S. Army Research Laboratory
Attn: AMSRL-WT-NF
2800 Powder Mill Road
Adelphi, MD 20783-1197

8. PERFORMING ORGANIZATION REPORT NUMBER
ARL-TR-302

9. SPONSORING/MONITORING AGENCY NAME(S) AND ADDRESS(ES)
U.S. Army Research Laboratory
2800 Powder Mill Road
Adelphi, MD 20783-1197

10. SPONSORING/MONITORING AGENCY REPORT NUMBER

11. SUPPLEMENTARY NOTES
AMS code: 611102.H4411
ARL PR: 4AE125

12a. DISTRIBUTION/AVAILABILITY STATEMENT
Approved for public release; distribution unlimited.

12b. DISTRIBUTION CODE

13. ABSTRACT *(Maximum 200 words)*

One of the necessary pieces of equipment needed for ultra-wideband (UWB) radio effects measurements is a suitable UWB field probe and radiating antenna. The conical monopole antenna (CMA) is an easy-to-fabricate, inexpensive, and useful UWB device that can be used for both of these applications. In this report we present information that should allow both antenna designers and users to quickly assemble a custom CMA to meet their design goals. A subjective explanation of the theory of operation is presented along with analytical expressions that predict the radiated and received pulse shapes. Experimental results are presented to verify the CMA theory of operation; these results also serve as an example of how UWB radiation can be monitored with a CMA during field measurements.

14. SUBJECT TERMS	15. NUMBER OF PAGES
Wide bandwidth probe, UWB antenna, conical monopole antenna	18
	16. PRICE CODE

17. SECURITY CLASSIFICATION OF REPORT	18. SECURITY CLASSIFICATION OF THIS PAGE	19. SECURITY CLASSIFICATION OF ABSTRACT	20. LIMITATION OF ABSTRACT
Unclassified	Unclassified	Unclassified	UL

Contents

Figures

1. Introduction

The key element of an impulse radiation or reception system is the ultra-wideband (UWB) antenna. A UWB transmitting antenna is also a necessary component for a photoconductive UWB pulser [1–3]. Anotner primary use of UWB antennas is for UWB system evaluations, in which the antenna may be used as an accurate field sensor.

The Fourier transform of an ideal electrical impulse function reveals that a radiated electromagnetic impulse contains frequency components throughout the entire electromagnetic spectrum. Hence, in UWB systems, an antenna is required whose characteristics are relatively independent of frequency over a large bandwidth. One such antenna is the conical monopole antenna (CMA).

Distinguishing characteristics of the CMA are its ease of fabrication and its axially independent radiation pattern, which may be desirable for various applications. Also, simple analytical expressions exist that predict radiated and received pulse shapes under certain conditions that are easily satisfied by the choice of the proper size of CMA. Furthermore, by adjusting a single parameter (the cone angle), we can match the antenna to a wide variety of antenna feed impedance values.

A pair of CMA's can be fabricated at minimal cost in a machine shop with the use of a lathe, about $20 of copper material, and less than an hour of technician time. More importantly, the performance of the CMA as a receiving antenna can easily exceed that of a D-dot probe, which can cost several thousand dollars.

In this report we present a simple explanation of the operation of the CMA and provide some analytical expressions that allow one to determine radiated and received pulse shapes and energies under certain reasonable conditions. Results from some radiation and reception experiments are also presented that verify the theoretical development presented here.

In short, from the information given here, designers should be able to quickly and easily assemble conical antenna systems to meet their wide-band radiation and/or reception design goals.

2. Theory

The CMA is shown in figure 1. The figure also shows a D-dot probe and a dipole antenna, which are often used in the same frequency regime as field probes. A schematic view of a CMA is shown in figure 2. The ground plane provides an image plane for the cone, making operation of this antenna similar to that of a biconical antenna.

Note that there are two primary design parameters, the cone angle θ and cone length l. We can develop a heuristic model of the conical antenna by treating the conical antenna as a transmission line with a characteristic impedance, Z_A, estimated by [4–5]

$$Z_A = \left(Z_o/2\pi\right) \ln\left[\cot(\theta/2)\right] , \tag{1}$$

where Z_o = 377 Ω is the characteristic impedance of free space.

As θ approaches zero, Z_A increases without bound. This limit corresponds to a monopole antenna above a ground plane. Thus, the resonant frequencies of the monopole are analogous to those of a transmission-line-tuned stub. The resonances occur when the monopole antenna length l is $(2n + 1)/4$ wavelengths, where n is an integer; the monopole therefore certainly does not exhibit a wide-band characteristic.

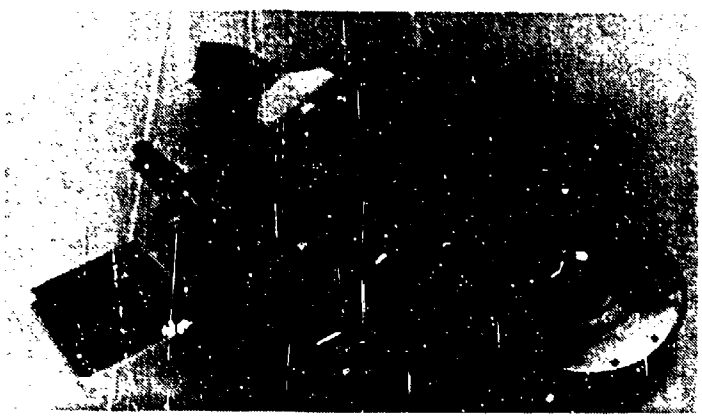

Figure 1. Conical monopole antenna (CMA) (left), shown with comparable dipole antenna (middle), and D-dot probe (right) for size comparison.

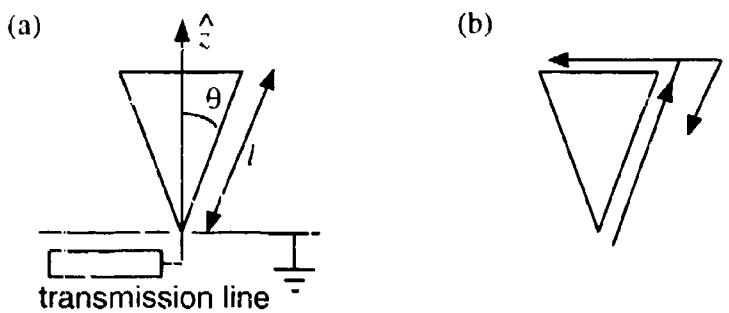

Figure 2. Conical monopole antenna: (a) geometry and (b) reflection at cone boundary.

On the other hand, one can design the CMA with a characteristic impedance that matches the source or feedline impedance by choosing the appropriate angle θ. Thus, an incident impulse or step-function waveform will propagate into the matched conical antenna with minimal reflection at the feedpoint.

Radiation of the incident pulse will then occur from two locations on the cone. These locations correspond to areas where charge is accelerated, a necessary condition for radiation. First, radiation occurs at the feedpoint as the incident pulse is launched onto the cone. Second, radiation occurs from the end of the cone, where the pulse is partially reflected and partially transmitted over the top of the cone, as shown in figure 2(b). We may analyze the expected shape of the pulse radiated or received by a CMA in the two limiting cases of a "long" or "short" CMA.

2.1 Radiation from a Long CMA and Matched Source

We define a "long" CMA as a CMA that is excited by a driving pulse with a pulse width significantly shorter than l/c, where l is the antenna length as shown in figure 2(a). First, consider the long transmitting antenna where Z_A is matched to the source. As a pulse from the source is launched into the antenna at the feedpoint, a temporal replica of the pulse is radiated according to [4]

$$E_Z^{rad}(t + r/c) = \frac{Z_o}{4\pi r Z_A} V_t(t) \ , \qquad (2)$$

where E_Z^{rad} is the electric field radiated on-axis and in the far field, r is the radius from the antenna source to the field point, and $V_t(t)$ represents the source voltage waveform. Note that the far field is polarized in the z-direction as defined in figure 2(a). Were the CMA infinitely long, this would be the only contribution to the radiated field, a desirable property since the temporal shape of the driving pulse is not distorted. One can achieve this condition artificially by providing resistive loading along the length of the cone, which attenuates the signal as it propagates away from the feedpoint, preventing further radiation at the endpoint of the cone [6].

In a practical CMA without resistive loading, the initial pulse of radiation is followed by additional radiation that occurs when the launched pulse reaches the end of the cone. Calculation of the radiation due to both reflection of the pulse back toward the source and transmission of the pulse over the top of the cone is a formidable task, and no analytical solution exists. However, if an antenna is designed with a large l, the second radiation event can be made to fall outside the time window of interest.

2.2 Radiation from a Short CMA and Matched Source

Now consider the radiated field produced when the CMA is "short" and Z_A is matched to the source impedance. The CMA is considered short if the driving pulse has a risetime and falltime much greater than l/c. In this regime, radiation occurs from both the feedpoint and the end of the cone simultaneously. In this case, the behavior of the CMA resembles that of a two-pole high-pass filter. The radiated field corresponds to the second derivative of the driving pulse as expressed by [4]

$$E_Z^{rad}(t + r/c) = \frac{Z_o}{Z_A} \frac{3l^2 \cos\theta}{4\pi r c^2} \frac{d^2 V_i(t)}{dt^2} \quad . \tag{3}$$

Therefore, a complete analytical solution for a short CMA exists; however, the actual pulse shape can be displayed only after a numerical integration is performed (fortunately, this is a simple and accurate process).

2.3 Reception with a CMA and Matched Load

It is not possible to perfectly reproduce the temporal shape of the radiated far field with a CMA used as a receiving antenna. But if the rise and fall times of the radiated pulse are long compared to l/c, the CMA may be regarded as short. An analytic expression for the received voltage, $V_r(t)$, at the matched load in this limit does exist and is given by [4]

$$V_r(t) = -\frac{3l^2 \cos\theta}{2c} \frac{dE_Z^{rad}(t)}{dt} \quad , \tag{4}$$

where $c = 3.0 \times 10^8$ m/s, and a matched load of impedance Z_A is assumed. The response mathematically resembles that of a single-time-constant high-pass filter that takes the first time derivative of the pulse. Similarly, if the CMA is long, the CMA behaves as a single-time-constant low-pass filter where an integral over time is taken. The received voltage at the matched load is given by [4]

$$V_r(t) = -\frac{c}{2} \int_{-\infty}^{t} E_Z^{rad}(t')\, dt' \quad . \tag{5}$$

Thus we see that useful expressions predicting the received voltage, as a function of the radiated electric field, exist and may easily be used to perform UWB field characterization. Furthermore, the frequency-domain response can be calculated from the Fourier transform of these equations.

3. CMA Transmission and Reception Experiments

Several CMA's were fabricated in Cu, each with a half-cone angle of $\theta = 47°$ and a corresponding characteristic impedance of 50 Ω. The antennas were characterized in the frequency domain with a scalar network analyzer (SNA) and in the time domain via an electro-optically produced short electrical pulse. The results presented here correspond to a CMA of length $l = 2.7$ cm, putting the antenna in the short antenna regime for frequency $f << 11$ GHz, and in the long antenna regime for $f >> 11$ GHz.

3.1 Frequency-Domain Measurements

The return loss, S_{11}, of the antenna was measured with a Wiltron 5447A SNA and is shown in figure 3. The decrease in return loss with increasing frequency at low frequencies corresponds to the first derivative action of the CMA, as expected from equation (2).

S_{21} transmission measurements were also completed (fig. 4) for the specific case of identical transmitting and receiving CMA's separated by $r = 12$ cm. At the low end of the spectrum, where both antennas are in the short antenna regime, the spectrum is characterized by a rapid increase in transmission with respect to frequency due to triple differentiation; the radiating antenna performs a double differentiation, while the receiving antenna performs a single differentiation. Note that the transmission spectrum is constant to within ±5 dB over more than an octave above 6 GHz.

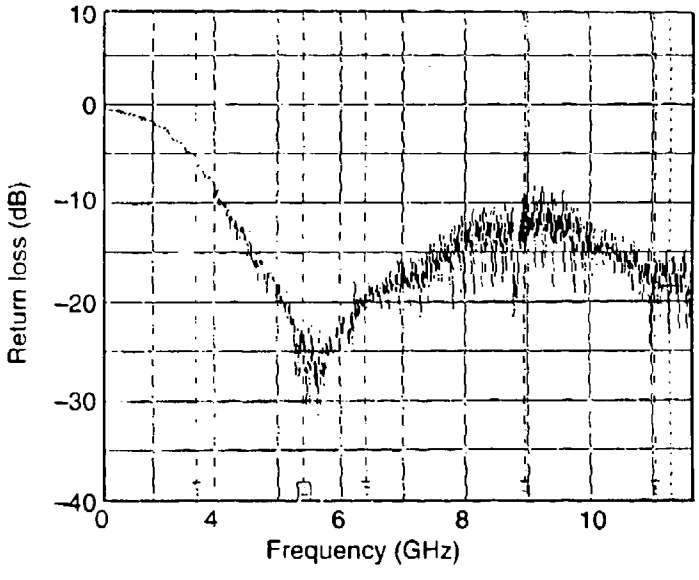

Figure 3. CMA return loss (S_{11}) measurement.

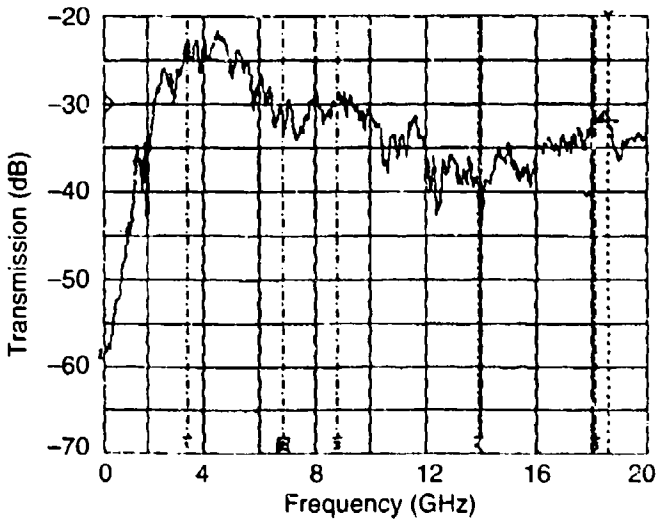

Figure 4. CMA transmission (S_{21}) measurement.

3.2 Time-Domain Measurements

The time-domain measurement involved producing a square-pulse excitation via a novel opto-electronic technique [7]. Briefly, the technique employs a high-T_c (critical temperature) superconductor (HTS) opening switch that is activated by a short (<100-ps pulse width) Nd:glass laser pulse. The experimental setup is shown in figure 5. While the HTS is in its normal zero-resistance state, the current source charges the shorted transmission line to the current I_0. When the HTS is activated by the laser pulse, it suddenly opens, producing a fast-risetime (~100 ps) pulse in the matched load. This pulse is shown in figure 6(a). The matched load is replaced by the l = 1.6 cm CMA so that the energy can be radiated. A D-dot probe was initially used to monitor the radiated field, but no signal was detected; the probe was replaced by another CMA, which was used as a receiving antenna. The setup is shown in figure 5(b).

The received pulse shape (fig. 6(b)) vividly illustrates that the combined effect of the transmitting and receiving CMA's is to take the third derivative of the square pulse used to excite the antennas. This result is completely consistent with equations (3) and (4).

3.3 Frequency-Domain Calculations

Often it is desirable to obtain the frequency spectrum of the received pulse so that we can assess the ultra-wideband performance of a system under test. This may be accomplished through a fast Fourier transform (FFT) algorithm. FFT algorithms are available as a part of a wide variety of software packages.

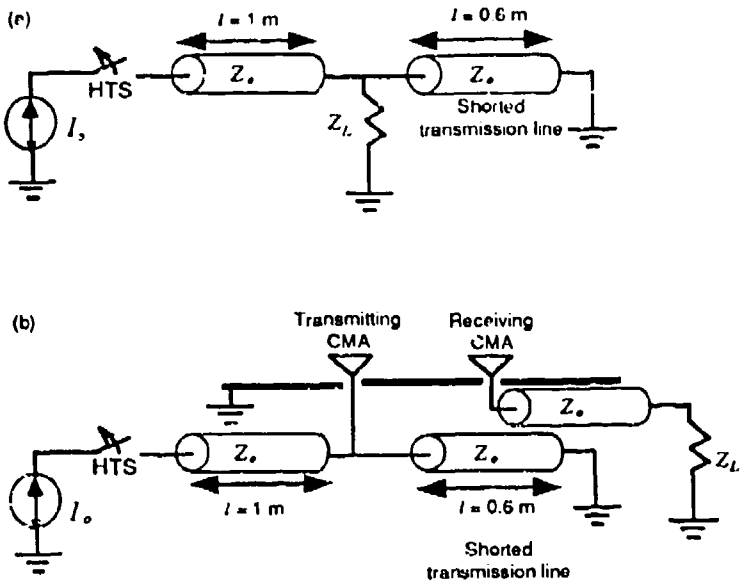

Figure 5. Setup for time-domain measurement using high-temperature superconductor (HTS). $Z_L = Z_o = 50\ \Omega$. (a) Pulse delivered to matched load, (b) pulse transmitted and received using CMA's.

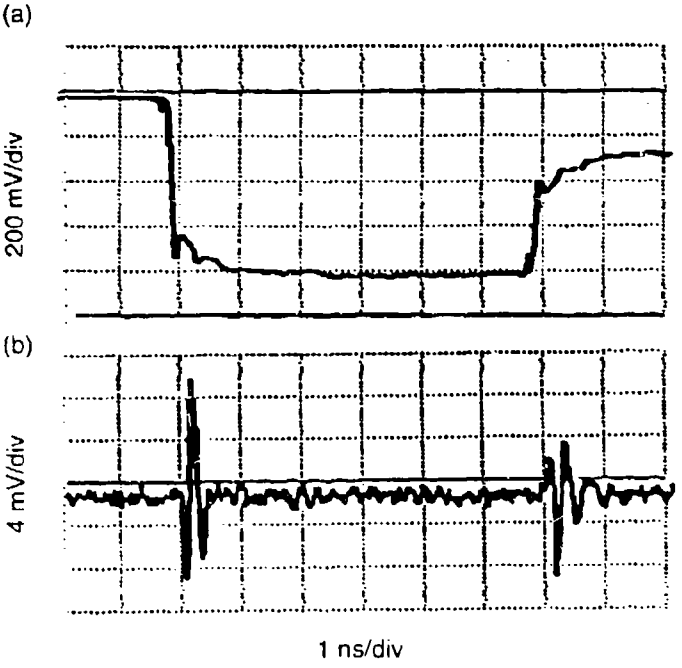

Figure 6. Pulse shapes used in time-domain measurements: (a) pulse delivered to load with setup of fig. 5(a); (b) transmitted and received pulse with setup of fig. 5(b).

Implementing the algorithm typically involves sampling the time-domain waveform at a specific time interval, Δt. The sampling interval must be less than half the reciprocal of the highest frequency contained in the waveform; this is a consequence of the Nyquist criterion. In addition, a pulsed waveform must be sampled over a time interval that is significantly longer than the pulse width. One usually lengthens this time interval by padding the data file with zeros, which would correspond to a null signal outside the time window

for which data are available. In practice, we found that the time interval over which the signal is sampled should be at least four times greater than the pulse width.

If there are N sample points, the FFT algorithm will then create a new array V_n, of either N or $N/2$ points (check the manual on your software package). The spectral density function $V_r(f)$ may be plotted with respect to frequency f as follows:

$$\begin{aligned} \left| V_r(t) \right| &= \Delta t \left| V_n \right| , \\ f &= n/\Delta t N . \end{aligned} \tag{6}$$

Frequencies corresponding to $n > N/2$ are disregarded, since they do not satisfy the Nyquist criterion. Other normalization constants may be needed; for specific details, check the manual on the software package.

Finally, one may plot the power spectrum of the received pulse (fig. 7) by squaring the spectral density function, $V_r(f)$, and dividing by the load impedance R_L. The units of this graph will be energy per unit bandwidth. The area under this power-spectrum curve must equal the total energy dissipated in the load, which is also the area under the curve: $V_r(t)^2/R_L$ versus t. Thus, one can calibrate the units of the power-spectrum curve by comparing these two areas.

To graph the spectrum of the field $E(t)$, rather than the received waveform $V_r(t)$, one can apply the frequency-domain versions of equations (4) or (5) to the frequency-domain graph. For instance, for a short antenna,

$$V_r^2(f) = \left| \frac{3l^2 \cos\theta}{c} \pi f \right|^2 E^2(f) . \tag{7}$$

Thus, the CMA combined with some simple software algorithms may be used in deducing the spectrum of the received field.

3.4 Antenna Pattern Measurements

Finally, the antenna pattern of the CMA was assessed. Measurements were completed on the 2.7-cm CMA at a frequency of 2.0 GHz (short CMA regime) in an anechoic chamber. The normalized plot of the V-polarized radiation pattern is given in figure 8. As expected, nulls exist at 0°, where radiation is shadowed by the top of the cone, and at 180°, where radiation is shadowed by the ground plane. The peak field is measured at an elevation angle coincident with the cone angle of ~47°.

Figure 7. Power spectrum of received pulse derived via a fast Fourier transform (FFT) of received pulse.

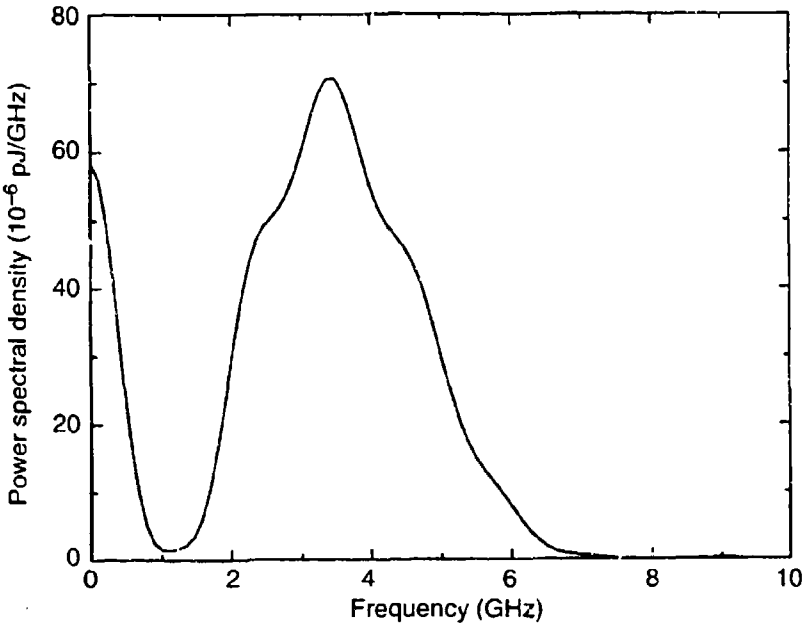

Figure 8. Normalized CMA (l = 2.7 cm) vertically polarized antenna pattern measured at 2.0 GHz. Orientation of CMA is shown at center. Measured field polarization is indicated by arrows.

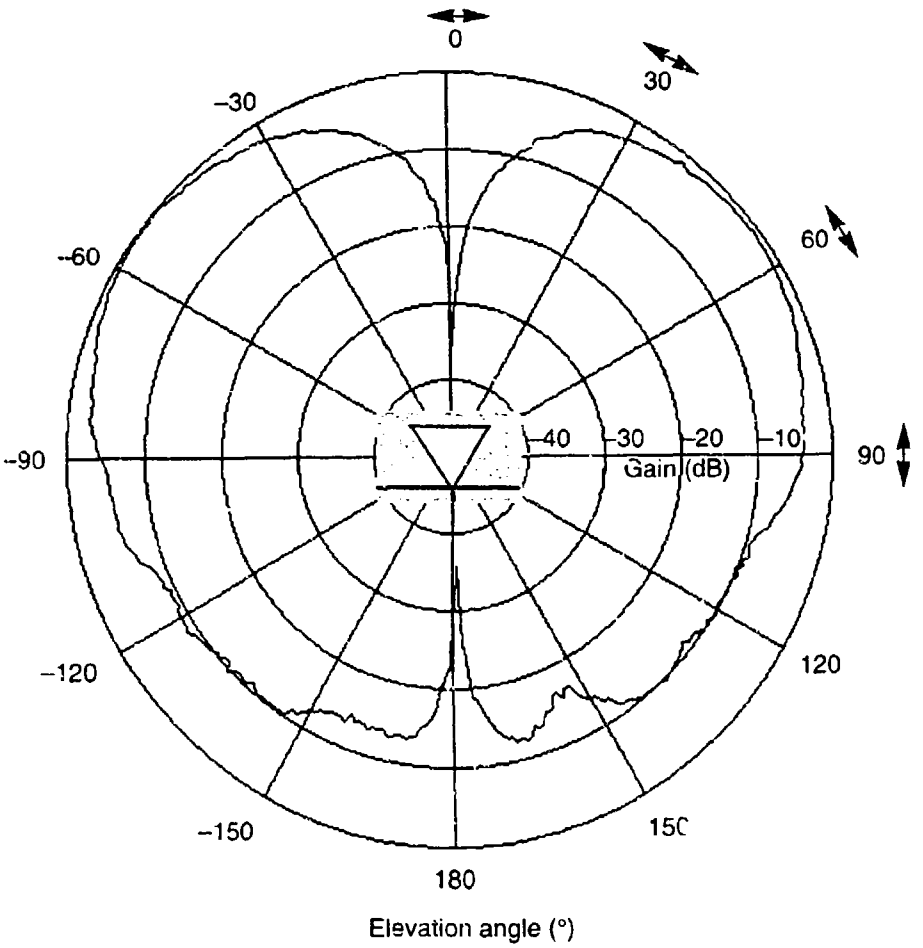

4. Conclusion

This experimental work verifies that, indeed, the CMA is a viable antenna for both transmission and reception of UWB electromagnetic pulses. This antenna has two primary advantages over other wideband antennas. First, the simple antenna geometry makes the CMA easy and inexpensive to fabricate, and by simply choosing the proper cone angle, one can design the CMA to match a wide variety of feedline impedances. Second, by judicious choice of antenna length, the antenna can be operated in either the "short antenna" or "long antenna" regime. In both these regimes, simple analytical expressions exist for the radiated and received signals. Thus, measured waveforms can easily be converted into equivalent measurements of the field being probed by simple integration or differentiation. One can also easily determine the spectrum of the received field by using an FFT on the received waveform and multiplying by a simple scaling factor.

Acknowledgment

The authors would like to thank Louis Jasper, Jr., for his support and Yi-Sern Lai and Prof. Chi H. Lee at the University of Maryland for their assistance in this work.

Literature Cited

1. E. E. Funk, C. C. Kung, E. A. Chauchard, M. J. Rhee, and Chi H. Lee, "Photoconductive switch controlled inductive pulsed power system," in *High power optically activated solid state switches*, Arye Rosen and Fred Zutavern, eds., Artech House, Norwood, MA (1993).

2. C. H. Lee, E. E. Funk, and L. J. Jasper, Jr., "High-power, compact, ultra-wideband pulser," *Proc. Second International Conference on Ultra-wideband Short Pulse Electromagnetics* (5–7 April 1994).

3. G. Arjavalingam, Yvon Pastol, Jean-Marc Habout, and Gerard V. Kopcsay, "Broad-band microwave measurements with transient radiation from optoelectronically pulsed antennas," *IEEE Trans. Microwave Theory Tech.* **MTT-38** (1990), 615–621.

4. C. W. Harrison, Jr., and C. S. Williams, Jr., "Transients in wide-angle conical antennas," *IEEE Trans. Antennas Propag.* **AP-13** (1965), 236–246.

5. J. D. Krauss, *Antennas*, McGraw Hill, New York (1988).

6. James G. Maloney and Glenn S. Smith, "Optimization of a conical antenna for pulse radiation: An efficient design using resistive loading," *IEEE Trans. Antennas Propag.* **AP-41** (1993), 940–947.

7. Y. S. Lai, E. E. Funk, W. L. Cao, Chi H. Lee, Zhi-Yaun Shen, Philip Pang, Denis J. Kountz, and William Holstein, "Ultra-wideband pulse generation and radiation using a high T_c superconductor opening switch," *Appl. Phys. Lett.* **65** (1994), 1048–1050.

Bibliography

Giorgio Franceschetti and Charles H. Papas, "Pulsed antennas," *IEEE Trans. Antennas Propag.* **AP-22** (1974), 651–661.

Paul E. Mayes, "Frequency-independent antennas and broad-band derivatives thereof," *Proc. IEEE* **80** (1992), 103–112.

C. A. Balanis, *Antenna theory: Analysis and design*, Wiley, New York (1982).

Distribution

Admnstr
Defns Techl Info Ctr
Attn DTIC-DDA (2 copies)
Cameron Sta Bldg 5
Alexandria VA 22304-6145

Advned Rsrch Proj Agcy
Attn DSO B Hui
3701 N Fairfax Dr
Arlington VA 22203

HQ
Dfns Nuc Agcy
Attn RAEE G Baker
6801 Telegraph Rd
Alexandria VA 22310-3398

Ofc of the Secy of Defs
Attn ODDRE/R & AT S Gontarek
The Pentagon
Washington DC 20301

Army Matl Comnd
Attn AMCRD-AR J Aveta
Attn AMCDE-PQI J Kreck
5001 Eisenhower Ave
Alexandria VA 22333-0001

Belvoir Rsrch Dev & Engrg Ctr
Attn STRBE-NA S Schaedel
FT Belvoir VA 22060-5606

HQ Dept of the Army
Dep Chf of Staf Oprs & Plns
Attn DAMO-FDI LTC R Morton
Room 2C536 The Pentagon
Washington DC 20310-0460

Hdqtr US Army Cmmctn-Elect Cmnd RD&E Ctr Night Vsn & Elect Sensors Directrt
Attn AMSEL-RD-NV-ADS M Kovach
FT Monmouth NJ 07703-5206

Ofc of the Assist Scy of the Army for Rsrch Dev & Acqstn
Attn SARD-TT F Milton
Rm 3E479 The Pentagon
Washington DC 20310-0103

Ofc of the Assist Secy of the Army for Rsrch Dev & Acqstn
Attn SARD-TT C Nash RM 3E411
Attn SARD-DOV LTC B Adams RM 3E479
Washington DC 20310-0103

US Army CECOM Intllgnc/Elect Warfare Drctrt
Attn AMSEL-RD-IEW-SPO D Helm
Vint Hill Farm Sta
Warrenton VA 22186-5100

Commandant
US Army Infantry Schl
Attn ATSH-CDM-E K Sines
FT Benning GA 31905-5400

US Army Mis Cmnd
Attn AMSMI-RD-WS-UB D'Holder
Redstone Arsenal AL 35898-8000

US Army Prgm Mgr—Firefinder
Attn SFAE-IEW-FF A Dirienzo
FT Monmouth NJ 07703-5305

US Army Sp & Strtgc Dfse Comnd
Attn CSSD-SL-S R Berg
PO Box 1500
Huntsville AL 35807-3801

Commander
US Army TRADOC
Attn ATCD-T J M Gray
FT Monroe VA 23651

Distribution

Nvl Rsrch Lab
Attn Code 4650 T Wieting
4555 Overlook Avenue SW
Washington DC 20375-5000

Sp & Nav Warfare Systs Comnd
Attn SPAWAR 332 J Albertine
2451 Crystal Park
Arlington VA 22245-5200

Air Force Phillips Lab
Attn PL/WSH H Dogliani
Attn PL/WSH M Harrison
Attn PL/WSH S Mason
Attn PL/WSH W Snyder
3550 Aberdeen Ave SE
Kirtland AFB NM 87117-6008

US Army Rsrch Lab
Attn AMSRL-WT D Hisley
Aberdeen Proving Ground MD 21005-5066

US Army Rsrch Lab
Attn AMSRL-OP-SD-TA Mail & Records Mgmt
Attn AMSRL-OP-SD-TL Tech Library (3 copies)
Attn AMSRL-OP-SD-TP Tech Pub
Attn AMSRL-PB-P L Weinberger
Attn AMSRL-SS-SG J McCorkle
Attn AMSRL-WT-NA R A Kehs
Attn AMSRL-WT-NF E Funk (12 copies)
Attn AMSRL-WT-NF E Scannell
Attn AMSRL-WT-NF L Jasper
Attn AMSRL-WT-NF R Kaul
Attn AMSRL-WT-NF S Saddow (12 copies)
Attn AMSRL-WT-NF T Bock
Attn AMSRL-WT-NH G Huttlin
Attn AMSRL-WT-NH J Corrigan